INTERNATIONAL JOURNAL FOR NUMERICAL METHODS IN ENGINEERING, VOL. 20, 2253–2281 (1984)

A TOTAL LAGRANGIAN FORMULATION FOR THE GEOMETRICALLY NONLINEAR ANALYSIS OF STRUCTURES USING FINITE ELEMENTS. PART I. TWO-DIMENSIONAL PROBLEMS: SHELL AND PLATE STRUCTURES

J. OLIVER AND E. OÑATE

E.T.S. Ingenieros de Caminos, Jorge Girona Salgado 31, Barcelona, Spain

SUMMARY

A total Lagrangian finite element formulation for the geometrically nonlinear analysis (large displacement/large rotations) of shells is presented. Explicit expressions of all relevant finite element matrices are obtained by means of the definition of a local co-ordinate system, based on the shell principal curvature directions, for the evaluation of strains and stresses. A series of examples of nonlinear analysis of shell and plate structures is given.

INTRODUCTION

The development of new and efficient formulations for nonlinear analysis of structures has attracted the study of many researchers in the past few years, and different alternative formulations have been presented recently.[1–7,11,16,19,21,22]. From the various structural types existing, especial interest has been focused on the numerical study of shell-plate or arch-beam structures, due mainly to the fact that most real engineering structural problems can be included into one of those two categories.

The present work fails within such a context of research, and can be classified as another effort to try to find a 'simple' and 'economical' formulation for the analysis of shell, plate, beam or arch-type structures which allows for geometrical nonlinearities due to the existence of large displacement/large rotations in the structure.

The formulation uses two-dimensional 'degenerated shell' finite elements[6] for the study of three-dimensional shells and plates, and one-dimensional elements for the analysis of arch, beam and axisymmetric shell structures. A total Lagrangian approach has been chosen for the definition of the deformation process of the structure.

Stress and strains are defined with respect to a local co-ordinate system *intrinsic* to the structure. In the case of shells, the co-ordinate axes coincide with the principal curvature directions and the normal vector at each point. *Explicit forms* of most finite element matrices can be obtained in a straightforward manner, as will be detailed later.

Normals to the midsurface before deformation are assumed to remain straight, but not necessarily normal to the midsurface after deformation, thus allowing for shear deformation effects. Moreover, zero elongation of the normal during deformation is strictly considered. Finally, it is

0029–5981/84/12 2253–29$02.90

Received 23 May 1983
Revised 16 November 1983

also worth noting that no restrictions are made on the magnitude of the shell curvatures. This might be of special interest for the analysis of non-shallow shells using a relatively small number of elements.

In this paper, the two-dimensional formulation to deal with three-dimensional shell (plate) problems is presented. Part two of this work dealing with one-dimensional structural problems (axisymmetric shells, arches and beams) will be published shortly.

In the first part of the paper the general finite element formulation for geometrically nonlinear analysis of shells is presented in detail and explicit expressions for most finite element matrices are given. Then, a series of examples of nonlinear analysis of shell and plate problems is presented.

GEOMETRIC DESCRIPTION

The middle surface of a general shell structure, such as the one shown in Figure 1, can be expressed in parametric form[20] as

$$\mathbf{r}_0 = \begin{Bmatrix} x_0(\mu_1, \mu_2) \\ y_0(\mu_1, \mu_2) \\ z_0(\mu_1, \mu_2) \end{Bmatrix} \tag{1}$$

In equation (1) μ_1 (μ_2 = constant) and μ_2 (μ_1 = constant) are the principal curvature lines of the shell middle surface. These lines are orthogonal at each point.

At each point, O, of the middle surface, unit vectors **a** and **b** tangent to curvature lines μ_1 and μ_2 in O, respectively, and **n** normal to the middle surface in O, are defined. Also, parameters r, s and t will be defined as the lengths measured along lines μ_1 and μ_2 and along the normal direction, **n**, respectively.

A second set of orthogonal vectors **l**, **m** and **n** can be defined at each point, as shown in Figure 2, in a way such that vector **l** is taken as parallel to the global plane xz and tangent to the shell middle surface, **n** is the normal vector, previously defined, and **m** is orthogonal to the plane **n**–**l**, and also tangent to the shell middle surface at point O. Note that, due to their definition, vectors **l** and **m** are not unit vectors, and their modulus is $e = (1 - n_y^2)^{1/2}$.

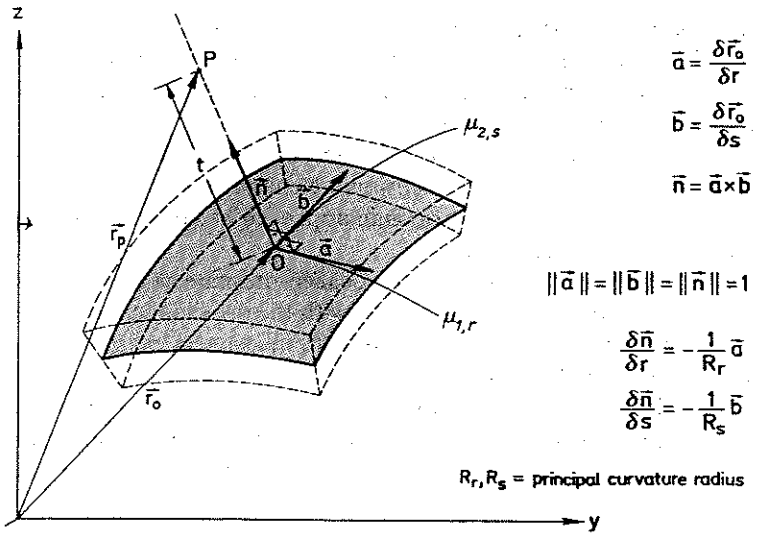

Figure 1. Definition of vectors **a**, **b** and **n**

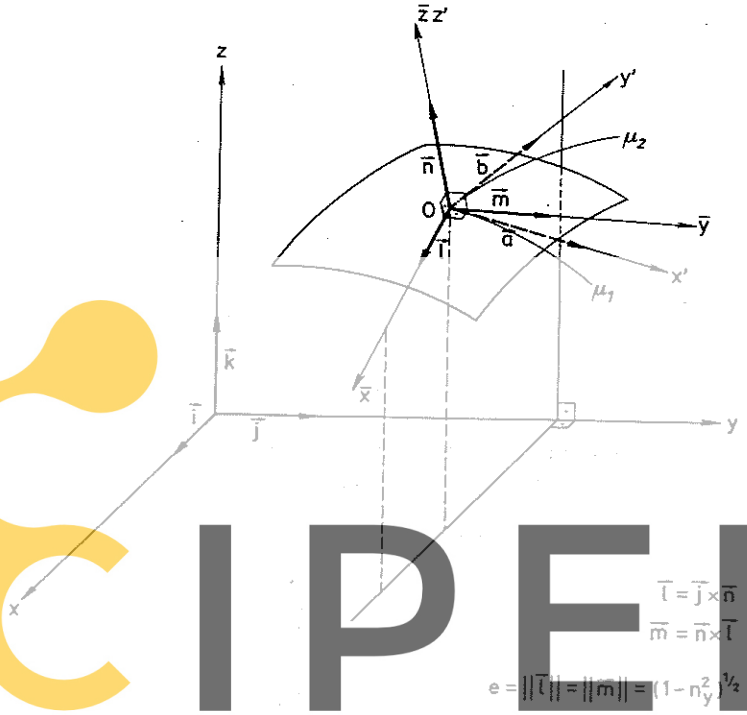

Figure 2. Definition of vectors l and m

The components of vectors **a**, **b**, **n**, **l** and **m** in the global reference system x, y, z (with associated unit vectors **i**, **j**, **k**, respectively, see Figure 2) can be written in matrix form as

$$\mathbf{a}=\begin{Bmatrix}a_x\\a_y\\a_z\end{Bmatrix}\quad \mathbf{b}=\begin{Bmatrix}b_x\\b_y\\b_z\end{Bmatrix}\quad \mathbf{n}=\begin{Bmatrix}n_x\\n_y\\n_z\end{Bmatrix}\quad \mathbf{l}=\begin{Bmatrix}l_x\\l_y\\l_z\end{Bmatrix}\quad \mathbf{m}=\begin{Bmatrix}m_x\\m_y\\m_z\end{Bmatrix} \tag{2}$$

where indices x, y and z refer to components associated to unit vectors **i**, **j** and **k**, respectively.

It can be seen in Figure 2 that vectors **a**, **b** and **n** define a set of local axes x', y' and z', associated with the shell principal curvature lines and their normal vector, respectively. On the other hand, vectors **l**, **m** and **n** define a second set of axes $\bar{x}$, $\bar{y}$ and $\bar{z}$, which although it can also be considered as 'local', is more easily identified within the structure ($\bar{x}$ is parallel to plane xz, etc.).

A point over the shell middle surface can be defined by a vector **r** (see Figure 1) such that

$$\mathbf{r}=\mathbf{r}_p=\mathbf{r}_0+t\cdot\mathbf{n} \tag{3}$$

or

$$\mathbf{r}=\begin{Bmatrix}x\\y\\z\end{Bmatrix}=\mathbf{r}_0(r,s)+t\cdot\mathbf{n}(r,s) \tag{4}$$

Using equation (4) and the relationships shown in Figure 1, the Jacobian matrix of the transformation $xyz\rightarrow rst$ can be written as

$$\left[\frac{\partial(x,y,z)}{\partial(r,s,t)}\right]=\left[\frac{\partial\mathbf{r}}{\partial r},\frac{\partial\mathbf{r}}{\partial s},\frac{\partial\mathbf{r}}{\partial t}\right]=\mathbf{T}^{\mathrm{T}}\cdot\mathbf{R} \tag{5}$$

where $\mathbf{T}$ is the orthogonal Jacobian matrix of the transformation $x'y'z' \rightarrow xyz$ given by

$$\mathbf{T} = \left[\frac{\partial(x'y'z')}{\partial(x,y,z)}\right] = \begin{bmatrix}\mathbf{a}^{\mathrm{T}}\\ \mathbf{b}^{\mathrm{T}}\\ \mathbf{n}^{\mathrm{T}}\end{bmatrix} = \begin{bmatrix}a_x & a_y & a_z\\ b_x & b_y & b_z\\ n_x & n_y & n_z\end{bmatrix} \tag{6}$$

and

$$\mathbf{R} = \left[\frac{\partial(x',y',z')}{\partial(r,s,t)}\right] = \begin{bmatrix}1-\dfrac{t}{R_r} & 0 & 0\\ 0 & 1-\dfrac{t}{R_s} & 0\\ 0 & 0 & 1\end{bmatrix} \tag{7}$$

is the Jacobian matrix of the transformation $x', y', z' \rightarrow r, s, t$.

Another matrix of special interest is that defining the components of vectors $\mathbf{l}$, $\mathbf{m}$ and $\mathbf{n}$ in the system $\mathbf{a}$, $\mathbf{b}$ and $\mathbf{n}$. From the definition of these vectors (see Figure 2) it is easy to obtain

$$[\mathbf{l}, \mathbf{m}, \mathbf{n}] = [\mathbf{a}, \mathbf{b}, \mathbf{n}] \cdot \mathbf{T} \tag{8}$$

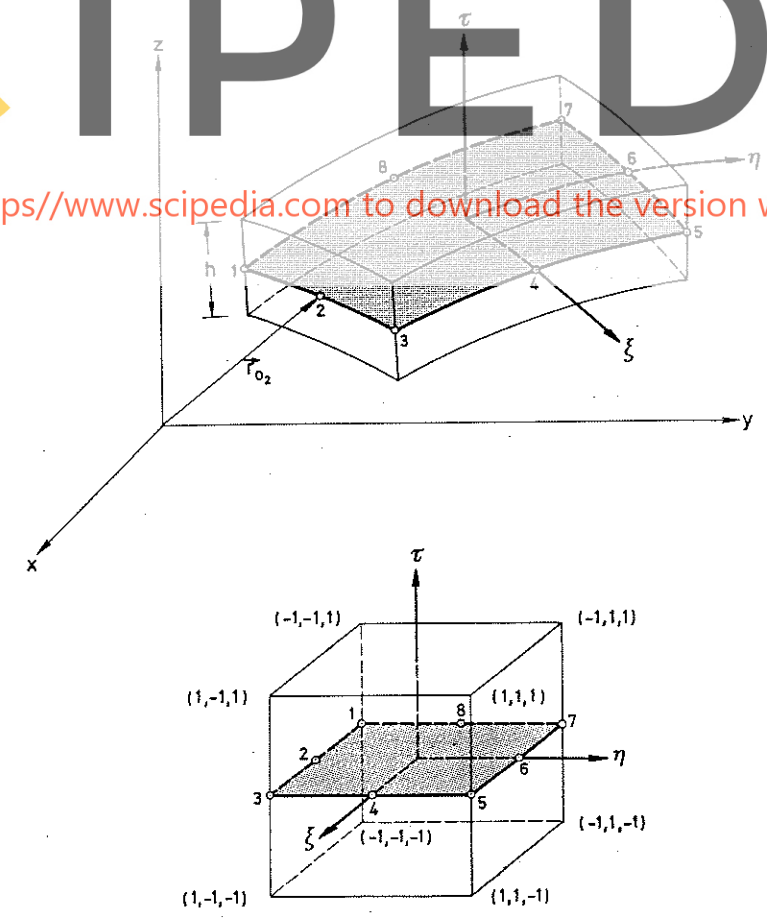

Figure 3. Typical eight-node isoparametric element. Normalized co-ordinate system and associated normalized volume

with

$$\bar{\mathbf{T}} = \begin{bmatrix} b_y & a_y & 0 \\ -a_y & b_y & 0 \\ 0 & 0 & 1 \end{bmatrix} \tag{9}$$

It is now possible to define the shell geometry in an approximate isoparametric form[24] as

$$\mathbf{r} = \sum_{1}^{n_e} N_i(\xi,\eta)\mathbf{r}_{0_i} + \tau\frac{h}{2}\mathbf{n}(\xi,\eta) \tag{10}$$

where $\mathbf{r}_{0_i}$ is the position vector of each node of a mesh of finite elements discretizing the shell middle surface (Figure 3), n_e the number of nodes of each element, N_i the shape function of node i, ξ and η the normalized isoparametric co-ordinates over the shell midsurface, and τ the third normalized co-ordinate. This τ co-ordinate is defined as

$$\tau = 2t/h \tag{11}$$

where h is the thickness of the element. Finally, the normal vector $\mathbf{n}(\xi,\eta)$ of equation (10) can be obtained from the approximate isoparametric middle surface and the expressions shown in Figure 1.

Equation (10) transforms the element volume into a cube of unit side defined in the co-ordinate system ξ, η, τ (see Figure 3).

KINEMATIC DESCRIPTION

The deformation of the shell is based on the following two main assumptions:

1. Normals to the shell middle surface before deformation remain straight, but not necessarily normal to the middle surface after deformation. This assumption has been frequently used in the context of linear and nonlinear analysis of 'thick' shells and plates by many authors.[1,6,10,15,19]
2. The length of the normal vector to the shell middle surface does not change during the deformation. This assumption, already suggested in alternative nonlinear shell formulations,[6] is strictly satisfied here by imposing that the unit length of the normal to the shell middle surface before deformation remains constant during the deformation process.

The first assumption allows to express the displacement vector $\mathbf{u}_1$ of a point P laying over the normal $\mathbf{n}$ at a distance t from the corresponding point O over the middle surface (see Figure 4), in terms of the displacement vector of point O, $\mathbf{u}_0$, and the relative displacement of the end of the normal vector in O, with respect to point P, $\mathbf{u}_1$, as

$$\mathbf{u} = \mathbf{u}_0 + t\mathbf{u}_1 \tag{12}$$

The vector of 'fundamental displacements' $\mathbf{p}$ is defined now as

$$\mathbf{p} = \{u_0, v_0, w_0, \bar{u}_1, \bar{v}_1, \bar{w}_1\}^{\mathrm{T}} \tag{13}$$

where u_0, v_0, w_0 are the components of $\mathbf{u}_0$ in the global system $\mathbf{i}$, $\mathbf{j}$, $\mathbf{k}$, and $\bar{u}_1$, $\bar{v}_1$, $\bar{w}_1$ are the components of $\mathbf{u}_1$, in the system $\mathbf{l}$, $\mathbf{m}$, $\mathbf{n}$, previously defined (see Figure 4).

Vector $\mathbf{p}$ defines generically the displacement of any point of the shell and it can be interpolated, within each element of the finite element mesh, in terms of its nodal values $\mathbf{p}_i$ as

$$\mathbf{p}(\xi,\eta) = \sum_{1}^{n_e} \mathbf{N}_i(\xi,\eta)\cdot\mathbf{p}_i \quad \mathbf{N}_i = N_i\cdot\mathbf{I}_6 \tag{14}$$

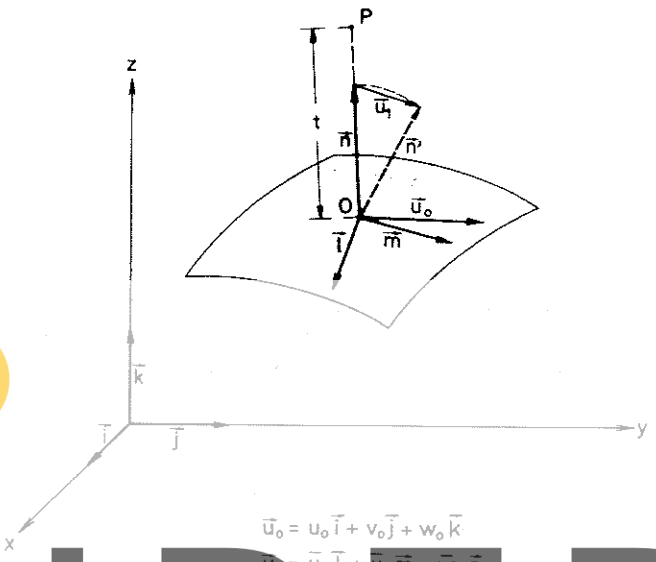

$$\bar{u}_o = u_o\,\bar{i} + v_o\,\bar{j} + w_o\,\bar{k}$$

$$\bar{u}_1 = \bar{u}_1\,\bar{t} + \bar{v}_1\,\bar{m} + \bar{w}_1\,\bar{n}$$

$$\underline{u}_o = \{u_o, v_o, w_o\}^T$$

$$\underline{u}_1 = \{\bar{u}_1, \bar{v}_1, \bar{w}_1\}^T$$

Figure 4. Definition of displacements

where $\mathbf{I}_6$ is a 6×6 unit matrix and

$$\mathbf{p}_i = \{u_{0_i}, v_{0_i}, w_{0_i}, \bar{u}_{1_i}, \bar{v}_{1_i}, \bar{w}_{1_i}\}^T \tag{15}$$

is the value of $\mathbf{p}$ at node i.

On the other hand, the second assumption allows to express the displacements $\bar{u}_{1_i}$, $\bar{v}_{1_i}$ and $\bar{w}_{1_i}$, due to the rotation of the normal $\mathbf{n}$, at node i, in terms of the angles α_i and β_i, defined in Figure 5, as

$$\bar{\mathbf{u}}_{1_i} = \{\bar{u}_{1_i}, \bar{v}_{1_i}, w_{1_i}\}^T = \left\{\frac{-\sin\alpha_i\cos\beta_i}{e_i}, \frac{-\sin\alpha_i\sin\beta_i}{e_i}, \cos\alpha_i - 1\right\}^T \tag{16}$$

Figure 6(a) shows the relationship between angles α_i and β_i with the two components $\theta_{\bar{x}_i}$ and $\theta_{\bar{y}_i}$ of the rotation vector, $\boldsymbol{\theta}_i$, of point i, tangent to the middle surface at point i. Vector $\boldsymbol{\theta}_i$ expresses the anticlockwise rotation of the normal.

It is worth noting that equation (16) leads to the equality $\|\mathbf{n}_i'\| = \|\mathbf{n}_i + \mathbf{u}_{1_i}\| = 1$. This is consistent with the second assumption of zero elongation of the unit normal independently of the magnitude of the rotations (large rotations formulation). Also, equation (16) and the relationships shown in Figure 6, allow us to reduce to five the number of nodal displacement unknowns. Therefore, the vector of displacements for node i is simply

$$\mathbf{a}_i = \{u_{0_i}, v_{0_i}, w_{0_i}, \theta_{\bar{x}_i}\theta_{\bar{y}_i}\}^T \tag{17}$$

Finally, it is worth pointing out that the definition of rotations (and their associated bending moments), shown in Figure 6 (b), is consistent with the definition of the work of the bending moments obtained as a scalar product of vectors $\mathbf{M}_i$ and $\boldsymbol{\theta}_i$, i.e.

$$\mathbf{M}_i \cdot \boldsymbol{\theta}_i = M_{\bar{x}_i} \cdot \theta_{\bar{x}_i} + M_{\bar{y}_i} \cdot \theta_{\bar{y}_i} \tag{18}$$

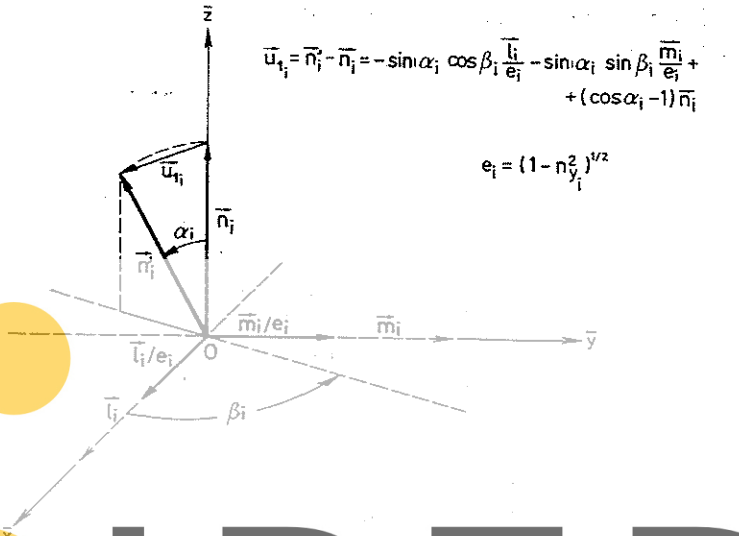

Figure 5. Definition of angles α_i and β_i

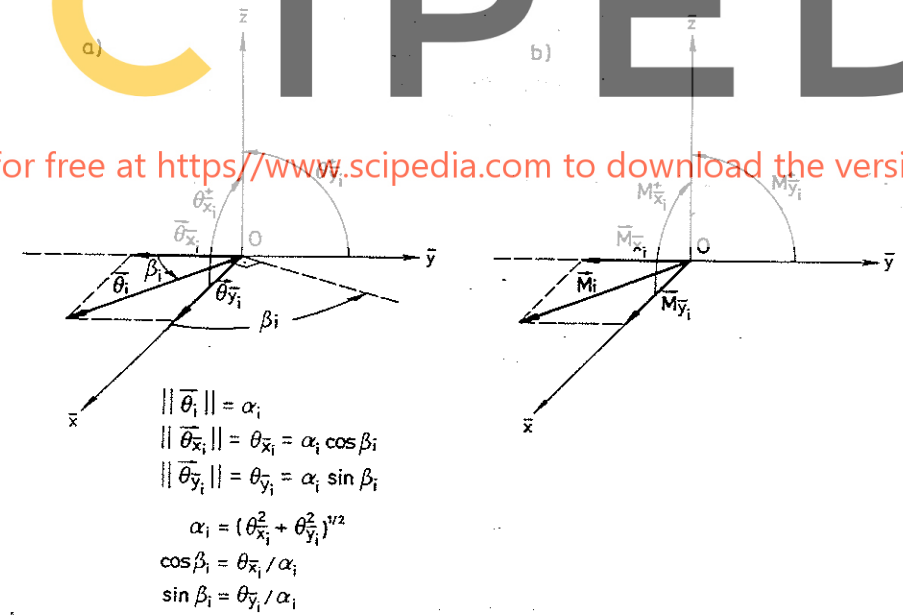

Figure 6. Sign convention for rotations and bending moments

STRAIN FIELD

Let us define $\mathbf{u}' = [u', v', w']^T$ as the vector containing the components of the displacement vector $\mathbf{u}$ of *any* point of the shell measured in the co-ordinate system defined by vectors $\mathbf{a}$, $\mathbf{b}$ and $\mathbf{n}$, corresponding at a *particular* point, O, laying over the shell middle surface, i.e.

$$\mathbf{u} = u'\mathbf{a} + v'\mathbf{b} + w'\mathbf{n} \tag{19}$$

The vector of displacement gradients at a point, P, laying over the normal vector in O (see Figure 4) can be defined now as

$$\mathbf{g} = \begin{Bmatrix} \mathbf{g}_1 \\ \mathbf{g}_2 \\ \mathbf{g}_3 \end{Bmatrix} \tag{20}$$

with

$$\mathbf{g}_1 = \begin{Bmatrix} g_1 \\ g_2 \\ g_3 \end{Bmatrix} = \begin{Bmatrix} \dfrac{\partial u'}{\partial x'} \\ \dfrac{\partial v'}{\partial x'} \\ \dfrac{\partial w'}{\partial x'} \end{Bmatrix}_P \quad \mathbf{g}_2 = \begin{Bmatrix} g_4 \\ g_5 \\ g_6 \end{Bmatrix} = \begin{Bmatrix} \dfrac{\partial u'}{\partial y'} \\ \dfrac{\partial v'}{\partial y'} \\ \dfrac{\partial w'}{\partial y'} \end{Bmatrix}_P \quad \mathbf{g}_3 = \begin{Bmatrix} g_7 \\ g_8 \\ g_9 \end{Bmatrix} = \begin{Bmatrix} \dfrac{\partial u'}{\partial z'} \\ \dfrac{\partial v'}{\partial z'} \\ \dfrac{\partial w'}{\partial z'} \end{Bmatrix}_P \tag{21}$$

where subscript P denotes values in point P.

Thus, the Green strain vector at point P (associated with the local directions x', y', z' of Figure 2) can be written using equation (21) as

$$\boldsymbol{\varepsilon} = \begin{Bmatrix} \varepsilon_{x'} \\ \varepsilon_{y'} \\ \gamma_{x'y'} \\ \gamma_{x'z'} \\ \gamma_{y'z'} \end{Bmatrix} = \begin{Bmatrix} g_1 + \frac{1}{2}(g_1^2 + g_2^2 + g_3^2) \\ g_5 + \frac{1}{2}(g_4^2 + g_5^2 + g_6^2) \\ g_2 + g_4 + g_1 g_4 + g_2 g_5 + g_3 g_6 \\ g_3 + g_7 + g_1 g_7 + g_2 g_8 + g_3 g_9 \\ g_6 + g_8 + g_4 g_7 + g_5 g_8 + g_6 g_9 \end{Bmatrix} \tag{22}$$

On the other hand, vector $\mathbf{g}$ can be obtained in terms of the fundamental displacement vector, $\mathbf{p}$, of equation (13) as (see Appendix I).

$$\mathbf{g} = \begin{Bmatrix} \mathbf{g}_1 \\ \mathbf{g}_2 \\ \mathbf{g}_3 \end{Bmatrix} = \mathbf{L} \cdot \mathbf{p} = \begin{bmatrix} C_r \mathbf{T} \dfrac{\partial}{\partial r} & tC_r \left(\boldsymbol{\Delta}_1 + \bar{\mathbf{T}} \dfrac{\partial}{\partial r} \right) \\ C_s \mathbf{T} \dfrac{\partial}{\partial s} & tC_s \left(\boldsymbol{\Delta}_2 + \bar{\mathbf{T}} \dfrac{\partial}{\partial s} \right) \\ \mathbf{0} & \bar{\mathbf{T}} \mathbf{1} \end{bmatrix} \begin{pmatrix} \mathbf{u}_0 \\ \bar{\mathbf{u}}_1 \end{pmatrix} \tag{23}$$

with

$$C_r = \frac{1}{1 - t/R_r} \tag{24}$$

$$C_s = \frac{1}{1 - t/R_s} \tag{25}$$

$$\boldsymbol{\Delta}_1 = \frac{1}{R_r} \begin{bmatrix} 0 & n_y & -1 \\ -n_y & 0 & 0 \\ b_y & a_y & 0 \end{bmatrix} \tag{26}$$

$$\boldsymbol{\Delta}_2 = \frac{1}{R_s} \begin{bmatrix} n_y & 0 & 0 \\ 0 & n_y & -1 \\ -a_y & b_y & 0 \end{bmatrix} \tag{27}$$

Substituting equation (14) in equation (23) it can be finally written

$$\mathbf{g} = \mathbf{L} \cdot \sum_{1}^{n_e} \mathbf{N}_i \cdot \mathbf{p}_i = \sum_{1}^{n_e} \mathbf{M}_i \cdot \mathbf{p}_i \tag{28}$$

where

$$\mathbf{M}_i = \begin{bmatrix} C_r \mathbf{T} \dfrac{\partial N_i}{\partial r} & tC_r \left(N_i \boldsymbol{\Delta}_1 + \dfrac{\partial N_i}{\partial r} \bar{\mathbf{T}} \right) \\ C_s \mathbf{T} \dfrac{\partial N_i}{\partial s} & tC_s \left(N_i \boldsymbol{\Delta}_2 + \dfrac{\partial N_i}{\partial s} \bar{\mathbf{T}} \right) \\ \underbrace{\mathbf{0}}_{\bar{M}_i} & \underbrace{N_i \cdot \bar{\mathbf{T}}}_{\bar{\bar{M}}_i} \end{bmatrix} = [\bar{M}_i, \bar{\bar{M}}_i] \tag{29}$$

Computation of the strain increment vector

Taking into account the linearity of $\mathbf{M}_i$, we can write from equation (28) that

$$\delta \mathbf{g} = \sum_{1}^{n_e} \mathbf{M}_i \delta \mathbf{p}_i \tag{30}$$

Using the expressions of Figure 6 and differentiating equation (16) a relationship between fundamental displacement and nodal displacement increments at a node can be found in the form

$$\delta \mathbf{p}_i = \mathbf{C}_i \cdot \delta \mathbf{a}_i \tag{31}$$

where

$$\mathbf{C}_i = \begin{bmatrix} \mathbf{I}_3 & \mathbf{0} \\ \mathbf{0} & \mathbf{V}_i \end{bmatrix} \qquad \mathbf{V}_i = \begin{bmatrix} V_{1i} & V_{2i} \\ V_{2i} & V_{3i} \\ V_{4i} & V_{5i} \end{bmatrix} \tag{32}$$

$$\begin{aligned} V_{1i} &= -\frac{1}{e_i} \left(\cos \alpha_i \cos^2 \beta_i + \frac{\sin \alpha_i}{\alpha_i} \sin^2 \beta_i \right) \\ V_{2i} &= -\frac{1}{e_i} \sin \beta_i \cos \beta_i \left(\cos \alpha_i - \frac{\sin \alpha_i}{\alpha_i} \right) \\ V_{3i} &= -\frac{1}{e_i} \left(\cos \alpha_i \sin^2 \beta_i + \frac{\sin \alpha_i}{\alpha_i} \cos^2 \beta_i \right) \\ V_{4i} &= -\sin \alpha_i \cos \beta_i \\ V_{5i} &= -\sin \alpha_i \sin \beta_i \end{aligned} \tag{33}$$

Thus, after substituting equation (31) in equation (30), we have

$$\delta \mathbf{g} = \sum_{1}^{n_e} \mathbf{M}_i \cdot \mathbf{C}_i \delta \mathbf{a}_i = \sum_{1}^{n_e} \mathbf{G}_i \delta \mathbf{a}_i \tag{34}$$

with

$$\mathbf{G}_i = \mathbf{M}_i \cdot \mathbf{C}_i = \begin{bmatrix} C_r \dfrac{\partial N_i}{\partial r} \mathbf{T} & tC_r \left[N_i \boldsymbol{\Delta}_1 + \dfrac{\partial N_i}{\partial r} \bar{\mathbf{T}} \right] \mathbf{V}_i \\ C_s \dfrac{\partial N_i}{\partial s} \mathbf{T} & tC_s \left[N_i \boldsymbol{\Delta}_2 + \dfrac{N_i}{\partial s} \bar{\mathbf{T}} \right] \mathbf{V}_i \\ \mathbf{0} & N_i \bar{\mathbf{T}} \mathbf{V}_i \end{bmatrix} \tag{35}$$

Table I. Matrix G_i

$$
\begin{array}{cccc}
C_r a_x \dfrac{\partial N_i}{\partial r} & C_r a_y \dfrac{\partial N_i}{\partial r} & C_r a_z \dfrac{\partial N_i}{\partial r} & tC_r\left(\dfrac{\partial N_i}{\partial r}(b_y V_{1_i} + a_y V_{2_i}) - \dfrac{N_i}{R_r}(V_{5_i} - n_y V_{2_i})\right) \\
C_r b_x \dfrac{\partial N_i}{\partial r} & C_r b_y \dfrac{\partial N_i}{\partial r} & C_r b_z \dfrac{\partial N_i}{\partial r} & tC_r\left(\dfrac{\partial N_i}{\partial r}(-a_y V_{1_i} + b_y V_{2_i}) - \dfrac{N_i}{R_r}(V_{6_i} - n_y V_{1_i})\right) \\
C_r n_x \dfrac{\partial N_i}{\partial r} & C_r n_y \dfrac{\partial N_i}{\partial r} & C_r n_z \dfrac{\partial N_i}{\partial r} & tC_r\left(\dfrac{N_i}{R_r}(b_y V_{1_i} + a_y V_{2_i}) + \dfrac{\partial N_i}{\partial r} V_{4_i}\right) \\
C_s a_x \dfrac{\partial N_i}{\partial s} & C_s a_y \dfrac{\partial N_i}{\partial s} & C_s a_z \dfrac{\partial N_i}{\partial s} & tC_s\left(\dfrac{\partial N_i}{\partial s}(b_y V_{1_i} + a_y V_{2_i}) + \dfrac{N_i}{R_s}(V_{6_i} - n_y V_{1_i})\right) \\
C_s b_x \dfrac{\partial N_i}{\partial s} & C_s b_y \dfrac{\partial N_i}{\partial s} & C_s b_z \dfrac{\partial N_i}{\partial s} & tC_s\left(\dfrac{\partial N_i}{\partial s}(-a_y V_{1_i} + b_y V_{2_i}) - \dfrac{N_i}{R_s}(V_{4_i} - n_y V_{2_i})\right) \\
C_s n_x \dfrac{\partial N_i}{\partial s} & C_s n_y \dfrac{\partial N_i}{\partial s} & C_s n_z \dfrac{\partial N_i}{\partial s} & tC_s\left(\dfrac{N_i}{R_s}(-a_y V_{1_i} + b_y V_{2_i}) + \dfrac{\partial N_i}{\partial s} V_{4_i}\right) \\
0 & 0 & 0 & N_i(b_y V_{1_i} + a_y V_{2_i}) \\
0 & 0 & 0 & N_i(-a_y V_{1_i} + b_y V_{2_i}) \\
0 & 0 & 0 & N_i V_{4_i}
\end{array}
$$

$$
V_{1_i} = -\frac{1}{e_i}\left(\cos\alpha_i \cos^2\beta_i + \frac{\sin\alpha_i}{\alpha_i}\sin^2\beta_i\right) \qquad V_{4_i} = -\sin\alpha_i \cos\beta_i
$$

$$
V_{2_i} = -\frac{1}{e_i}\left(\sin\alpha_i \cos\beta_i\left(\cos\alpha_i - \frac{\sin\alpha_i}{\alpha_i}\right)\right) \qquad V_{5_i} = -\sin\alpha_i \sin\beta_i
$$

$$
V_{3_i} = -\frac{1}{e_i}\left(\cos\alpha_i \sin^2\beta_i + \frac{\sin\alpha_i}{\alpha_i}\cos^2\beta_i\right)
$$

Equation (35) shows the nonlinearity of matrix $\mathbf{G}_i$ due to matrix $\mathbf{V}_i$ of equation (32), whose terms are functions of the nodal rotations. A more explicit form of matrix $\mathbf{G}_i$ is given in Table I. Additionally, details of the computation of the curvature radius and derivatives of shape functions, which appear in the expression of $\mathbf{G}_i$ of Table I, are given in Appendix II.

The relationship between Green strains and nodal displacement increments is obtained from equation (22) as

$$\delta\boldsymbol{\varepsilon} = \mathbf{A}\cdot\delta\mathbf{g} \tag{36}$$

with

$$\mathbf{A} = \begin{bmatrix} 1+g_1 & g_2 & g_3 & 0 & 0 & 0 & 0 & 0 & 0 \\ 0 & 0 & 0 & g_4 & 1+g_5 & g_6 & 0 & 0 & 0 \\ g_4 & 1+g_5 & g_6 & 1+g_1 & g_2 & g_3 & 0 & 0 & 0 \\ g_7 & g_8 & 1+g_9 & 0 & 0 & 0 & 1+g_1 & g_2 & g_3 \\ 0 & 0 & 0 & g_7 & g_8 & 1+g_9 & g_4 & 1+g_5 & g_6 \end{bmatrix} \tag{37}$$

and after substitution of equation (30) in (36) it can be finally written

$$\delta\boldsymbol{\varepsilon} = \mathbf{A}\cdot\sum_1^{n_e}\mathbf{G}_i\cdot\delta\mathbf{a}_i = \sum_1^{n_e}\mathbf{B}_i\delta\mathbf{a}_i \tag{38}$$

$$\mathbf{B}_i = \mathbf{A}\cdot\mathbf{G}_i \tag{39}$$

CONSTITUTIVE EQUATIONS

The second Piola–Kirchhoff stress vector, corresponding to the Green strain vector of equation (22), is defined now as

$$\boldsymbol{\sigma} = [\sigma_{x'}, \sigma_{y'}, \tau_{x'y'}, \tau_{x'z'}, \tau_{y'z'}]^{\mathrm{T}} \tag{40}$$

where x', y' and z' are the local axes defined in Figure 2.

The constitutive relationship *must* be incorporated to the general formulation in an incremental, or rate form, of the type

$$\delta\boldsymbol{\sigma} = \mathbf{D}^*\delta\boldsymbol{\varepsilon} \tag{41}$$

We will not go into details of the different forms of matrix $\mathbf{D}^*$ for the various types of material behaviour. A comprehensive study of the usually accepted constitutive equations for nonlinear structural analysis can be found in Reference 8.

DISCRETIZED EQUILIBRIUM EQUATIONS

The discretized equilibrium equations for the structure are derived via the virtual work expression which, in its finite element total Lagrangian form, can be written as[24]

$$\boldsymbol{\Psi}(\mathbf{a}) = \mathbf{P}(\mathbf{a}) - \mathbf{R}(\mathbf{a}) = 0 \tag{42}$$

which for the ith node gives

$$\boldsymbol{\Psi}_i(\mathbf{a}) = \int_V \mathbf{B}_i^{\mathrm{T}}\cdot\boldsymbol{\sigma}\,\mathrm{d}V - \mathbf{R}_i(\mathbf{a}) = \mathbf{0} \tag{43}$$

In equations (42), $\boldsymbol{\Psi}(a)$ is the residual force vector and $\mathbf{R}(a)$ is the equivalent nodal force vector due to exterior loads.

In this work the external loads have been assumed to be conservative. Therefore, vector $\mathbf{R}$ in

equation (42) can be taken as independent of the nodal displacements and equation (43) can be written as

$$\Psi_i(\mathbf{a}) = \int_V \mathbf{B}_i^{\mathrm{T}} \cdot \boldsymbol{\sigma} \mathrm{d}V - \mathbf{R}_i \tag{44}$$

Typical cases of external loads are as follows:

Point loads. For which vector $\mathbf{R}_i$ has the form

$$\mathbf{R}_i = [f_{x_i}, f_{y_i}, f_{z_i}, M_{\bar{x}_i}, M_{\bar{z}_i}]^{\mathrm{T}} \tag{45}$$

in which f_{x_i}, f_{y_i}, f_{z_i} are the point loads acting at node i along the global directions x, y, z, respectively, and $M_{\bar{x}_i}$ and $M_{\bar{y}_i}$ are the bending moments at node i of local axes $\bar{x}$ and $\bar{y}$, respectively.

Surface loads

$$\mathbf{R}_i = \int_{A^{(e)}} [N_i t_x, N_i t_y, N_i t_z, 0, 0]^{\mathrm{T}} \, \mathrm{d}r \, \mathrm{d}s \tag{46}$$

where t_x, t_y, t_z are the intensities of a uniform load acting over the element middle surface along the global directions x, y, z, respectively.

Self weight

$$R_i = -\int_{A^{(e)}} [0, 0, N_i, 0, 0]^{\mathrm{T}} \rho g h \mathrm{d}r \, \mathrm{d}s \tag{47}$$

where ρ is the element density, g the value of gravity (assumed to act along the vertical global axe z) and h the element thickness.

EQUATIONS SOLUTION METHOD— COMPUTATION OF THE TANGENT MATRIX

The solution of systems of equations like that of equation (42) for geometrically nonlinear structural problems, in which snap-through, snap-back, bifurcation, etc., phenomena might take place, has been the objective of numerous studies, and many solution strategies are available in the literature (i.e. standard or modified Newton–Raphson, quasi-Newton, BFGS, arc-length, conjugate gradient, creep-type methods, etc.).[25,26] In this work, one of the simplest procedures—the standard Newton–Raphson solution combined with a load incremental method—has been chosen. However, the formulation presented in the paper allows us to use any other solution strategy based on the knowledge of the residual force vector of equation (42) and the tangent matrix $\mathbf{K}_T = \partial \boldsymbol{\psi}(\mathbf{a})/\partial \mathbf{a}$.

In the Newton Raphson algorithm the incremental displacement vector, corresponding to the nth iteration, is calculated as

$$\Delta \mathbf{a}^n = -\mathbf{K}_T(\mathbf{a}^n) \boldsymbol{\Psi}(\mathbf{a}^n) \tag{48}$$

from which the updated displacement field can be computed as $\mathbf{a}^{n+1} = \mathbf{a}^n + \Delta \mathbf{a}^n$. A convergence criterion based on the comparison of the quadratic norm of the residual force vector $\boldsymbol{\psi}(\mathbf{a})$, with that of the vector of external forces $\mathbf{R}(\mathbf{a})$, has been chosen. The iterative process stops when the relation value between both norms is less than a prescribed value ε. (In the examples presented in this paper, the value of $\varepsilon = 1$ per cent has been taken.)

A typical sub-matrix of $\mathbf{K}_T$, linking nodes i and j, can be obtained by

$$\mathbf{K}_{T_{ij}}(\mathbf{a}) = \frac{\partial \boldsymbol{\Psi}_i(\mathbf{a})}{\partial \mathbf{a}_j} \tag{49}$$

Taking the first variation of equation (43), we obtain

$$\delta \boldsymbol{\Psi}_i(\mathbf{a}) = \sum_{j=1}^{n} \mathbf{K}_{T_{ij}} \cdot \delta \mathbf{a}_i = \int_V \delta \mathbf{B}_i^{\mathrm{T}} \cdot \boldsymbol{\sigma} \, \mathrm{d}V + \int_V \mathbf{B}_i^{\mathrm{T}} \delta \boldsymbol{\sigma} \, \mathrm{d}V \tag{50}$$

The second of the above integrals can be expressed, by making use of equations (38) and (41), as

$$\int_V \mathbf{B}_i^{\mathrm{T}} \cdot \delta \boldsymbol{\sigma} \, \mathrm{d}V = \sum_{j=1}^{n} \int_V \mathbf{B}_i^{\mathrm{T}} \mathbf{D}^* \mathbf{B}_j \, \mathrm{d}V \delta \mathbf{a}_j = \sum_{j=1}^{n} \mathbf{K}_{ij}^{L} \delta \mathbf{a}_j \tag{51}$$

with

$$\mathbf{K}_{ij}^{L} = \int_V \mathbf{B}_i^{\mathrm{T}} \mathbf{D}^* \mathbf{B}_j \, \mathrm{d}V \tag{52}$$

On the other hand, the first integral of the right-hand side of equation (50) can be written, using equation (39), as

$$\int_V \delta \mathbf{B}_i^{\mathrm{T}} \boldsymbol{\sigma} \, \mathrm{d}V = \int_V \mathbf{G}_i^{\mathrm{T}} \cdot \delta \mathbf{A}^{\mathrm{T}} \cdot \boldsymbol{\sigma} \, \mathrm{d}V + \int_V \delta \mathbf{G}_i^{\mathrm{T}} \cdot \mathbf{A}^{\mathrm{T}} \cdot \boldsymbol{\sigma} \, \mathrm{d}V \tag{53}$$

The above integrals can be transformed as follows. Using equations (37), (40) and (34) it can be written

$$\int_V \mathbf{G}_i^{\mathrm{T}} \delta \mathbf{A}^{\mathrm{T}} \boldsymbol{\sigma} \, \mathrm{d}V = \int_V \mathbf{G}_i^{\mathrm{T}} \cdot \mathbf{S} \cdot \delta \mathbf{g} \, \mathrm{d}V = \sum_{j=1}^{n} \int_V \mathbf{G}_i^{\mathrm{T}} \cdot \mathbf{S} \cdot \mathbf{G}_j \, \mathrm{d}V \delta \mathbf{a}_j = \sum_{j=1}^{n} \mathbf{K}_{ij}^{\sigma \mathrm{I}} \delta \mathbf{a}_j \tag{54}$$

with

$$\mathbf{K}_{ij}^{\sigma \mathrm{I}} = \int_V \mathbf{G}_i^{\mathrm{T}} \mathbf{S} \mathbf{G}_j \, \mathrm{d}V \tag{55}$$

where

$$\mathbf{S} = \begin{bmatrix} \sigma_{x'} \mathbf{I}_3 & \tau_{x'y'} \mathbf{I}_3 & \tau_{x'z'} \mathbf{I}_3 \\ \tau_{x'y'} \mathbf{I}_3 & \sigma_{y'} \mathbf{I}_3 & \tau_{y'z'} \mathbf{I}_3 \\ \tau_{x'z'} \mathbf{I}_3 & \tau_{y'z'} \mathbf{I}_3 & \mathbf{0} \end{bmatrix} \tag{56}$$

The second integral of the right-hand side of equation (56) can be written as

$$\int_V \delta \mathbf{G}_i^{\mathrm{T}} \cdot \mathbf{A}^{\mathrm{T}} \cdot \boldsymbol{\sigma} \, \mathrm{d}V = \sum_{j=1}^{n} \mathbf{K}_{ij}^{\sigma \mathrm{II}} \delta \mathbf{a}_j \tag{57}$$

Matrix $\mathbf{K}^{\sigma \mathrm{II}}$ of equation (57) can be simply obtained using the fact that $\mathbf{M}_i$ is independent of the nodal unknowns. Thus, it can be written, making use of equations (35), (32) and (29),

$$\delta \mathbf{G}_i^{\mathrm{T}} = \delta \mathbf{C}_i^{\mathrm{T}} \cdot \mathbf{M}_i^{\mathrm{T}} = \begin{bmatrix} \mathbf{0} & \mathbf{0} \\ \mathbf{0} & \delta \mathbf{V}_i^{\mathrm{T}} \end{bmatrix} \begin{bmatrix} \bar{\mathbf{M}}_i^{\mathrm{T}} \\ \bar{\mathbf{M}}_i^{\mathrm{T}} \end{bmatrix} = \begin{bmatrix} \mathbf{0} \\ \delta \mathbf{V}_i^{\mathrm{T}} \cdot \bar{\mathbf{M}}_i^{\mathrm{T}} \end{bmatrix} \tag{58}$$

Now, since matrix $\mathbf{V}_i$ is a function of the nodal rotations $\theta_{\bar{x}_i}$ and $\theta_{\bar{y}_i}$ only, it can be finally obtained

$$\mathbf{K}_{ij}^{\sigma \mathrm{II}} = \mathbf{0} \quad \text{for } i \neq j \tag{59}$$

$$\mathbf{K}_{ii}^{\sigma u}=\begin{bmatrix}0 & 0 & 0 & 0 & 0\\ 0 & 0 & 0 & 0 & 0\\ 0 & 0 & 0 & 0 & 0\\ 0 & 0 & 0 & H_{11} & H_{12}\\ 0 & 0 & 0 & H_{21} & H_{22}\end{bmatrix} \tag{60}$$

where

$$\begin{pmatrix}H_{11}\\ H_{21}\end{pmatrix}_i=\int_V \frac{\partial \mathbf{V}_i^{\mathrm{T}}}{\partial \theta_{\bar{x}_i}}\bar{\mathbf{M}}_i^{\mathrm{T}}\mathbf{A}^{\mathrm{T}}\boldsymbol{\sigma}\,\mathrm{d}V;\quad\begin{pmatrix}H_{12}\\ H_{22}\end{pmatrix}_i=\int_V \frac{\partial \mathbf{V}_i^{\mathrm{T}}}{\partial \theta_{\bar{y}_i}}\bar{\mathbf{M}}_i^{\mathrm{T}}\mathbf{A}^{\mathrm{T}}\boldsymbol{\sigma}\,\mathrm{d}V \tag{61}$$

An explicit form of $\partial \mathbf{V}_i/\partial\theta_{\bar{x}_i}$ and $\partial \mathbf{V}_i/\partial\theta_{\bar{y}_i}$ matrices is presented in Appendix III. There it can be seen that $H_{12}=H_{21}$ and, therefore, $\mathbf{K}_{ii}^{\sigma u}$ is a symmetric matrix.

From equations (51), (54) and (57) we can finally write the full tangent matrix as

$$\mathbf{K}_{T_{ij}}=\mathbf{K}_{ij}^{L}+\mathbf{K}_{ij}^{\sigma I}+\mathbf{K}_{ij}^{\sigma u} \tag{62}$$

where $\mathbf{K}_{ij}^{L}$, $\mathbf{K}_{ij}^{\sigma I}$ and $\mathbf{K}_{ij}^{\sigma u}$ are obtained by equations (52), (55) and (59)–(60) respectively.

EXTENSIONS FOR KINKED SHELLS

The shell formulation presented in previous sections is valid only for smooth shells. However, extensions to allow for kinks (folded plate structures) are simple. They only imply the adequate transformation of the two local rotations $\theta_{\bar{x}}$, $\theta_{\bar{y}}$ into the global co-ordinate system, so that at a common node all the nodal forces contributed by the different elements meeting at the node are assembled in the same global system. The number of nodal unknowns then increases from five to six due to appearance of an extra nodal rotation after the transformation process. Such transformation can be easily done by using, in the first place, matrix $\bar{\mathbf{T}}$ of equation (9) to transform the two local rotations from the **l**, **m**, **n** axes, where they are originally defined, to the **a**, **b**, **n** axes. Then, matrix $\mathbf{T}$ (see equation (6)) can be used for the final transformation into the global axes. It can be easily shown that

$$\bar{\boldsymbol{\theta}}_i=\begin{bmatrix}\theta_{\bar{x}_i}\\ \theta_{\bar{y}_i}\\ \theta_{\bar{z}_i}\end{bmatrix}=\mathbf{T}_i^{*}\begin{bmatrix}\theta_{x_i}\\ \theta_{y_i}\\ \theta_{z_i}\end{bmatrix}=\mathbf{T}_i^{*}\cdot\boldsymbol{\theta}_i \tag{63}$$

with

$$\mathbf{T}_i^{*}=\frac{1}{e_i}\begin{bmatrix}0 & -1 & 0\\ 1 & 0 & 0\\ 0 & 0 & 1\end{bmatrix}\bar{\mathbf{T}}_i^{\mathrm{T}}\cdot\mathbf{T}_i\begin{bmatrix}0 & 1 & 0\\ -1 & 0 & 0\\ 0 & 0 & 1\end{bmatrix} \tag{64}$$

where e_i is the scaling factor defined in Figure 5.

The tangent matrix after the transformation $\hat{\mathbf{K}}_T$, can be computed as

$$\hat{\mathbf{K}}_{T_{ij}}=\hat{\mathbf{T}}_i^{\mathrm{T}}\mathbf{K}_{T_{ij}}^{*}\hat{\mathbf{T}}_j$$

where

$$\hat{\mathbf{T}}_i=\begin{bmatrix}\mathbf{I}_3 & \mathbf{0}\\ \mathbf{0} & \mathbf{T}_i^{*}\end{bmatrix};\quad\mathbf{K}_{T_{ij}}^{*}=\begin{bmatrix}\mathbf{K}_{T_{ij}} & \mathbf{0}\\ \mathbf{0} & 0\end{bmatrix} \tag{65}$$

Some precautions must be taken if the above transformations are performed for nodes which lay on smooth zones of the shell, since singularity of matrix $\hat{\mathbf{K}}_T$ will arise in those cases. This can be avoided by a selective transformation of rotations in the adequate nodes only, or by inserting an arbitrary number in the zero pivot coefficient at the equation solution stage.[24]

NUMERICAL INTEGRATION AND CHOSEN FINITE ELEMENT

All the different integrals have been evaluated using a Gauss–Legendre numerical integration quadrature.

It is worth noting from (7) that for the volume integrals

$$dV = dx'dy'dz' = \left|\frac{\partial(x'y'z')}{\partial(r,s,t)}\right| drdsdt = \det|\mathbf{R}|\,drdsdt$$
$$= (1 - t/R_r)(1 - t/R_s)\,drdsdt \tag{66}$$

On the other hand, from equation (10) and (15),

$$drds = \left|\frac{\partial(r,s)}{\partial(\xi,\eta)}\right| d\xi d\eta = \left|\frac{\partial(x_0,y_0)}{\partial(\xi,\eta)}\right| \Big/ \left|\frac{\partial(x_0,y_0)}{\partial(r,s)}\right| d\xi d\eta \tag{67}$$

$$dt = \frac{h}{2} d\tau$$

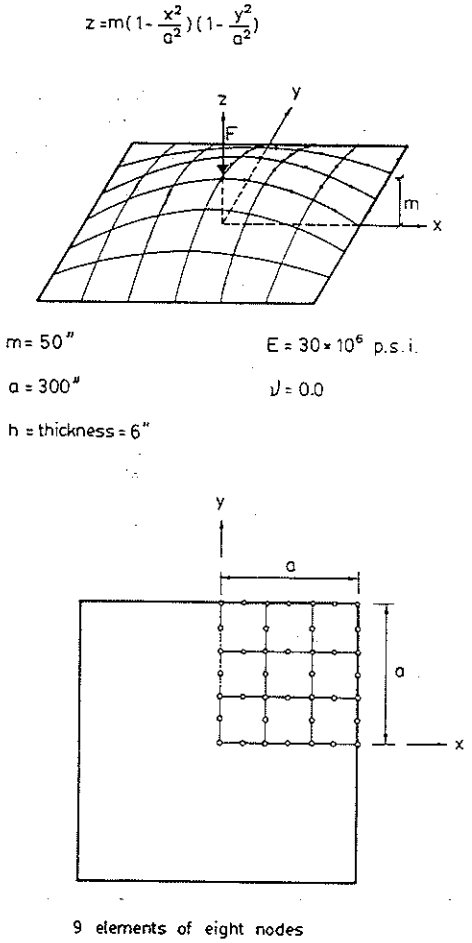

Figure 7. Parabolic shell under central point load. Geometry, material properties and finite element mesh used in the analysis

Thus, from (66) and (67),

$$dv = (1 - t/R_r)(1 - t/R_s)\frac{h}{2}\cdot\frac{\dfrac{\partial x_0}{\partial \xi}\cdot\dfrac{\partial y_0}{\partial \eta} - \dfrac{\partial x_0}{\partial \eta}\cdot\dfrac{\partial y_0}{\partial \xi}}{\dfrac{\partial x_0}{\partial r}\cdot\dfrac{\partial y_0}{\partial s} - \dfrac{\partial x_0}{\partial s}\cdot\dfrac{\partial y_0}{\partial r}}\cdot d\xi d\eta d\tau \tag{68}$$

Equation (68) allows the use of the normalized domain of Figure 3 for the numerical integration of all volume integrals.

With respect to the type of element chosen for the examples analysed, we have to note that the formulation presented here can, in fact, be classified within the range of 'thick shell formulations' and, therefore, any of the reduced integration family of elements recently developed to deal with thick/thin shells could be used.[6–13] For the examples presented in this paper, the eight-noded isoparametric element with the following integrating rule has been chosen:

1. Reduced integration (2×2 Gauss–Legendre rule) along directions ξ and η over the middle surface of the shell
2. A two-point integration rule over the thickness (τ direction) for the elastic solutions and 4–8 points for the elastoplastic solutions.

We are fully aware of some deficiencies found for this element in the range of very thin shells.[27] However, this element has been chosen here with the only objective of testing the formulation presented. Thus, all examples have been restricted to moderately thin shells. The numerical results obtained have been very accurate, as will be shown in next sections.

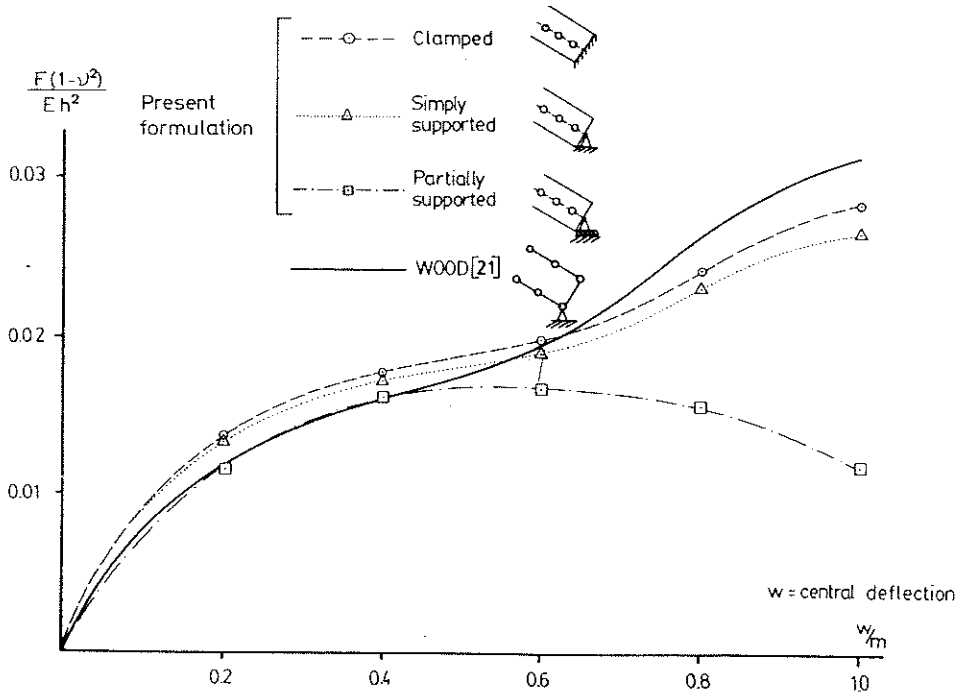

Figure 8. Parabolic shell. Normalized plot of the elastic central displacement versus for three different types of boundary conditions

NUMERICAL EXAMPLES

All the examples presented below have been solved in a VAX/VMS 11/780 computer using single precision.

Example 1. Parabolic shell–elastic analysis

The geometry of the shell and finite element mesh used can be seen in Figure 7. The problem has been analysed by a process of incrementing the central deflection from a zero initial value to a value of 50 in.

Numerical results obtained for the central displacement load elastic curve obtained for different types of boundary conditions at the shell edges are presented in Figure 8. Numerical results obtained by Wood with paralinear three-dimensional shell elements[21] are also shown for comparison. Note the differences between the boundary conditions imposed by Wood and those used in the present analysis.

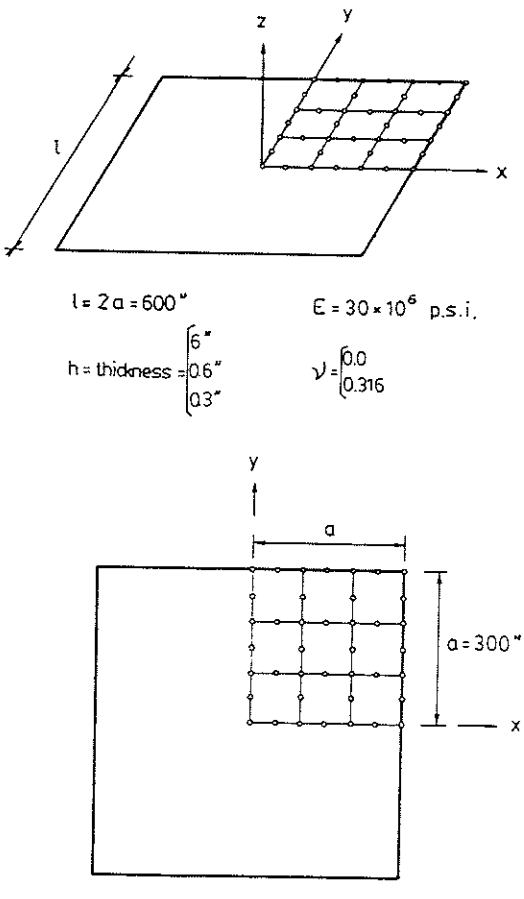

Figure 9. Simply-supported square plate. Uniform loading. Geometry, material properties and finite element mesh used in the analysis

Example 2. Simply-supported square plate—elastic analysis

In this example a simply-supported square plate under an increasing uniform vertical load has been analysed. The geometry of the plate, material properties and finite element mesh used can be seen in Figure 9. Note that only a quarter of the plate has been analysed due to symmetry. Numerical results obtained for the load intensity–central deflection elastic curve are plotted in

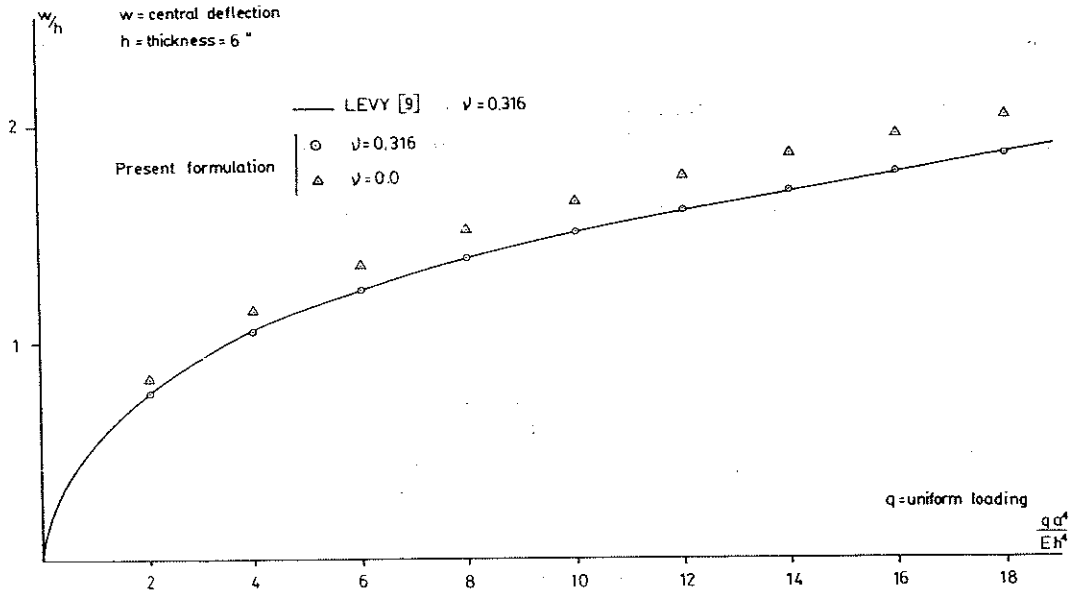

Figure 10. Simply-supported square plate. Normalized plot of the elastic central deflection versus load intensity for two different values of the Poisson ratio

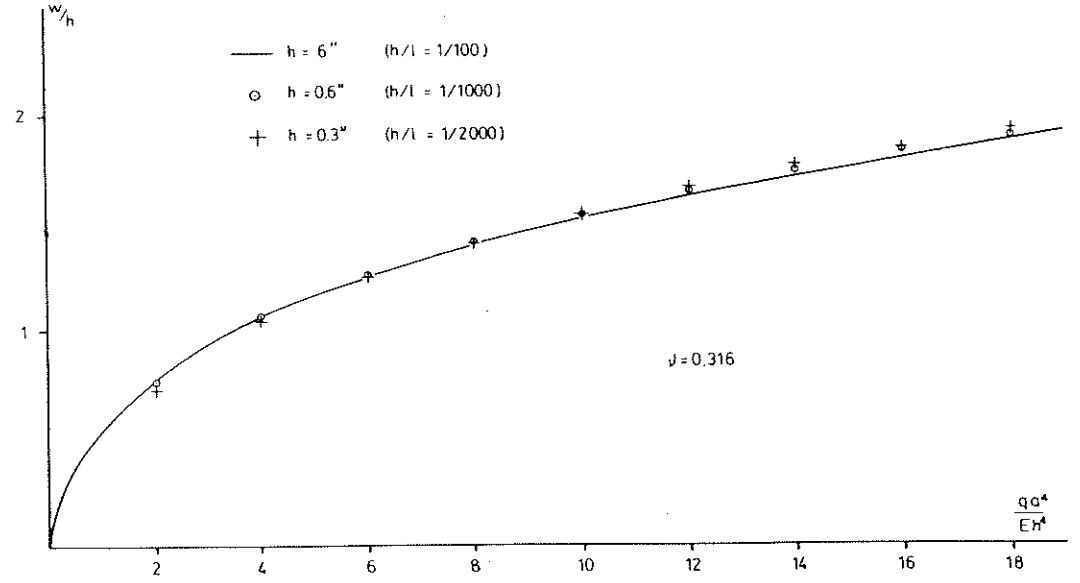

Figure 11. Simply-supported square plate. Normalized plot of the central deflection versus load intensity for three different thickness–width ratios

Figure 10, where results obtained by Levy[9] are also presented for comparison. Excellent agreement between the two solutions is obtained. Finally, the same problem has been analysed for different thickness–width ratios and numerical results for the load–deflection curve can be seen in Figure 11. It can be seen in these figures that the behaviour of the reduced integration eight-noded element used for the thick and moderately thin situations is good. Further research in this context for other different types of elements is actually on course.

Example 3. Cylindrical shell—elastic analysis

The cylindrical shell studied can be seen in Figure 12. Note that only four elements have been used to discretize one quarter of the structure (due to symmetry). The shell is assumed to be simply supported on its straight edges and free on the curved ones. In the analysis presented, an increasing

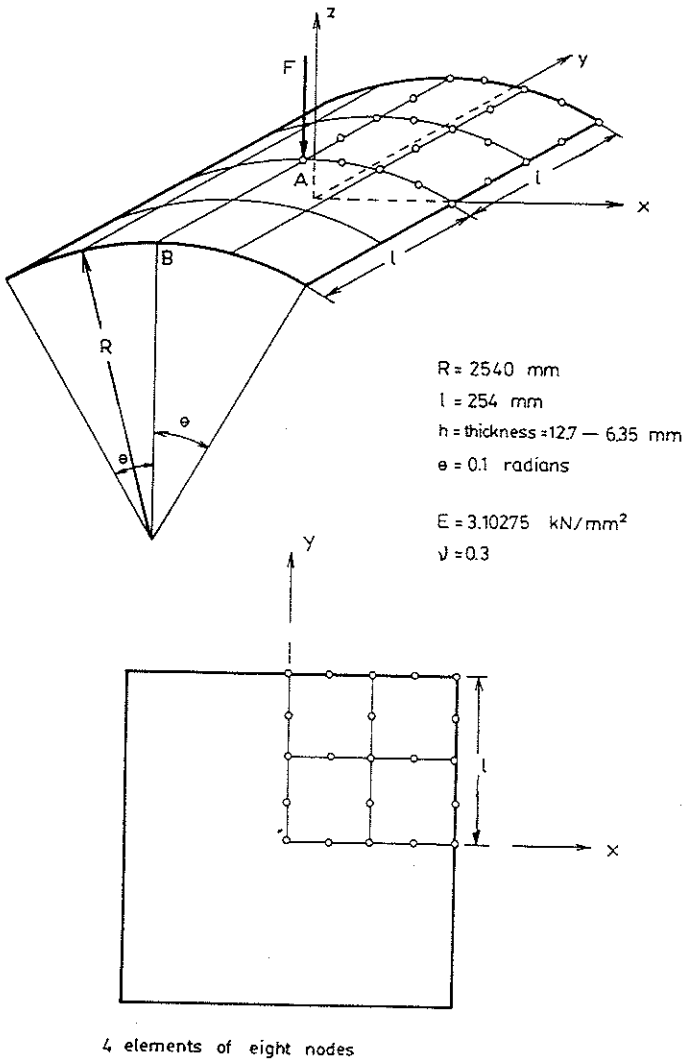

Figure 12. Cylindrical shell under central point load. Geometry, material properties and finite element mesh used in the analysis

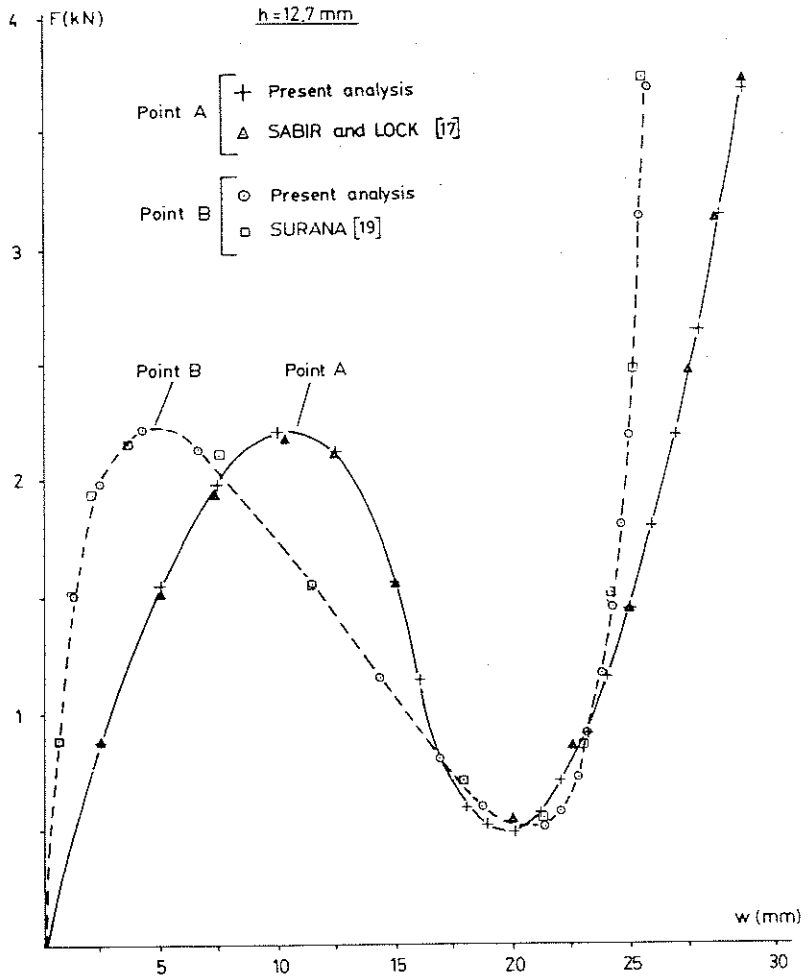

Figure 13. Cylindrical shell. Plot of the elastic deflection versus load for two different points of the shell for a thickness of 12·7 mm

displacement, w, is prescribed in point A and the corresponding vertical reaction force, F, obtained. In Figure 13, the load–deflection paths for points A (central) and B (mid-point of the free edge) for a shell thickness of 12·7 mm are presented. It can be seen that there is a snap-through point for a value of the force $F = 2{\cdot}2$ kN. The control of the vertical displacement of point A allows us to obtain all the load values along the deflection path. Numerical results agree well with those obtained by Sabir and Lock[17] and Surana.[19] When the shell thickness is reduced to half its value (6.35 mm) the load–deflection curve presents a snap-through point for $F \simeq 0.6$ kN, together with a snap-back one (vertical tangent) for a value of the deflection $w_p \simeq 17$ mm (see Figure 14). Numerical results show good agreement with those obtained by Sabir and Lock.[17] However, we have to note that the method of controlling the displacement of point A has a drawback for this particular case, since no results can be obtained in the region between the two vertical tangents. Results in that particular region can be obtained by using more sophisticated solution procedures,[25,26] as mentioned in the earlier section 'Equations solution method' which can be easily implemented in the shell formulation presented in this paper.

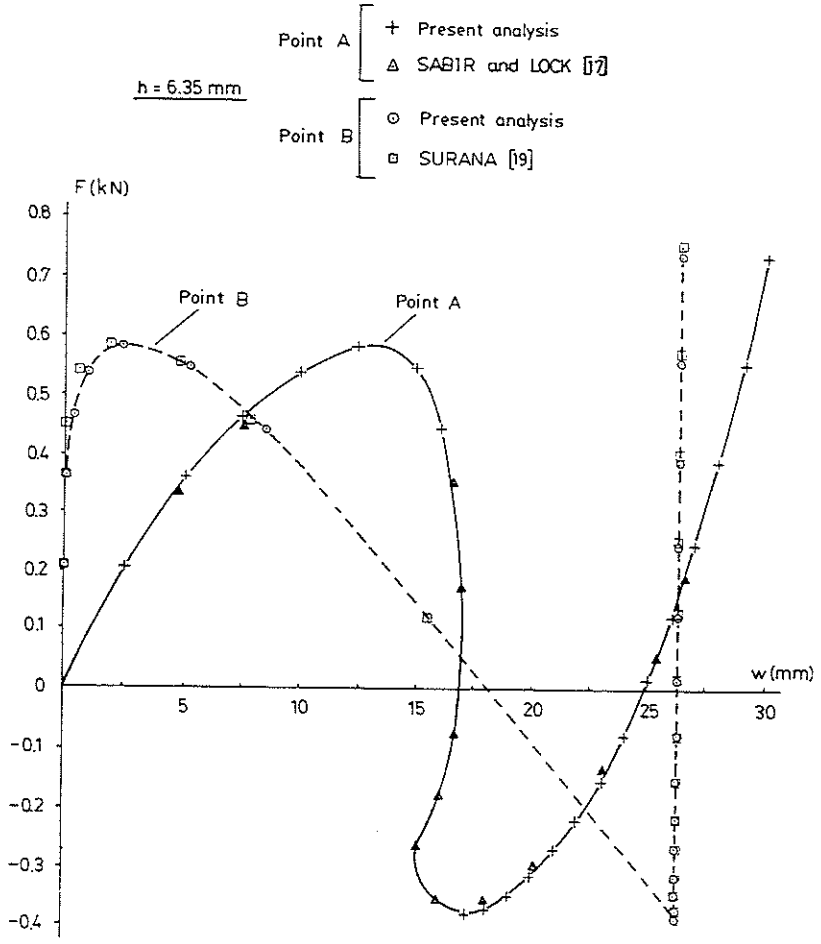

Figure 14. Cylindrical shell. Plot of the elastic deflection versus load for two different points of the shell for a thickness of 6·35 mm

Example 4. Spherical shell—elastic and elasto-plastic analysis

The last example is the analysis of a spherical shell with fully-clamped edges under an increasing vertical point load acting in the centre of the shell, as can be seen in Figure 15. Again, due to symmetry, only a quarter of the structure has been considered. A mesh of 7 eight noded elements has been used (see Figure 15). Results for the load–deflection at the centre have been plotted in Figure 16 for the elastic case and good agreement with results obtained by Wood with a two-dimensional axisymmetric formulation is obtained.

An elasto-plastic solution has also been attempted for the same problem. A Von Mises yield criteria with no strain hardening and an initial yield stress of 5×10^4 psi has been chosen. Numerical results for the elasto-plastic load–displacement curve for different integrating rules across the shell thickness are plotted in Figure 17. Finally, a drawing of the plastic zones for a central deflection of 0·16 in. is shown in Figure 18.

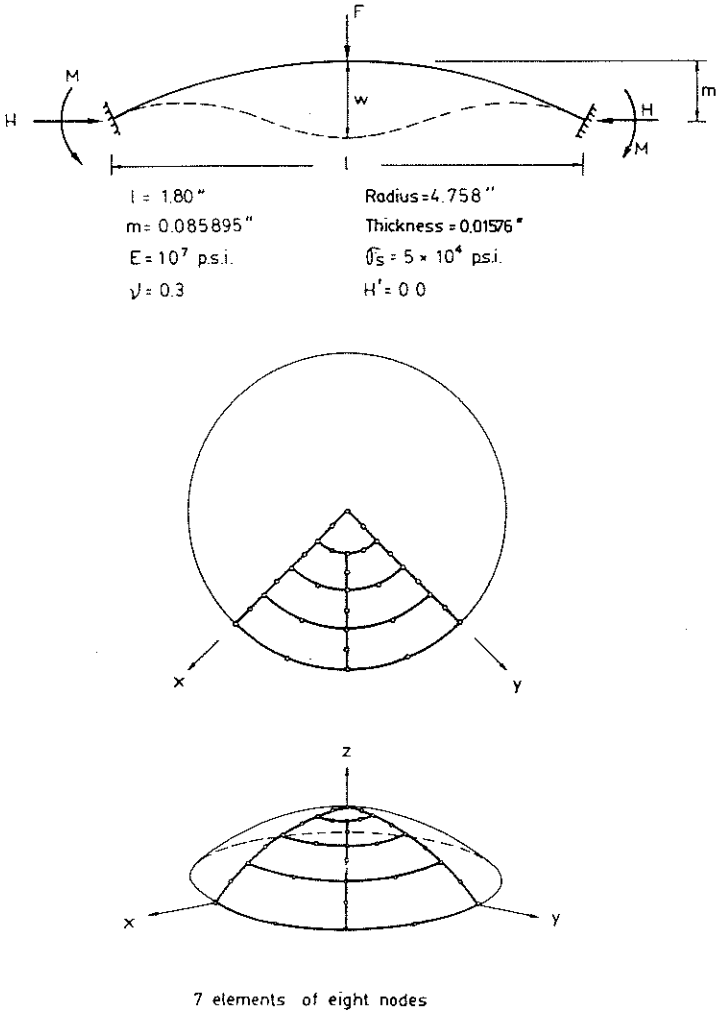

Figure 15. Spherical shell under point load. Geometry, material properties and finite element mesh used in the analysis

CONCLUSIONS

A total Lagrangian finite element formulation for the geometrically nonlinear analysis (large displacements/large rotations) of shells has been developed.

The formulation allows for large curvatures in the shell surface and shear deformation effects. Explicit forms of the relevant finite element matrices have been given. The formulation presented here is the basis for obtaining simpler formulations for the geometrical nonlinear analysis of different structural types, i.e., plates, axisymmetric shells, arches or beams. The accuracy of the formulation has been checked in a series of examples of nonlinear analysis of shell and plate structures. Details of the simplification of the shell formulation presented here, for the nonlinear analysis of 'one-dimensional' structures, together with further examples which will test the efficiency of the formulation, will be published shortly.

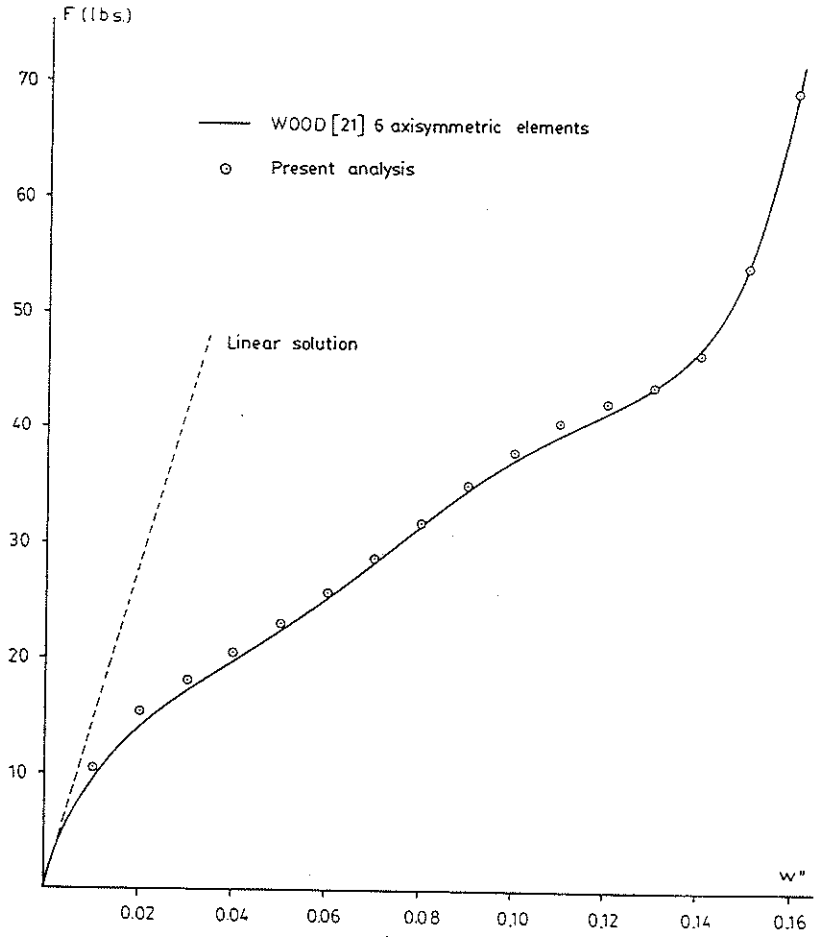

Figure 16. Spherical shell. Plot of the elastic central deflection versus load

APPENDIX I: COMPUTATION OF THE L OPERATOR

Let p be the shell point in which the **L** operator is to be calculated and O the corresponding point over the shell middle surface in which vectors $\mathbf{a}_0$, $\mathbf{b}_0$ and $\mathbf{n}_0$ and the local system of co-ordinates $x'y'z'$ are defined (see Figure 19).

Let Q be another point laying over the shell normal at a distance $\bar{t}$ from its corresponding point M over the shell midsurface (see Figure 19) and let $\mathbf{l}$, $\mathbf{m}$ and $\mathbf{n}$ be the vectors defined in point M, as explained in the second section. Let finally

$$\mathbf{u}'_Q = \mathbf{u}'_M + t^* \mathbf{u}'_{1M} \tag{69}$$

be the displacement vector of point Q in the system $x'y'z'$.

On the other hand, from equations (21) and (17) it can be deduced that

$$\mathbf{g}_1 = \left(C_r \frac{\partial \mathbf{u}'}{\partial r} \right)_p ; \mathbf{g}_2 = \left(C_s \frac{\partial \mathbf{u}'}{\partial s} \right)_p ; \mathbf{g}_3 = \left(\frac{\partial \mathbf{u}'}{\partial t} \right)_p \tag{70}$$

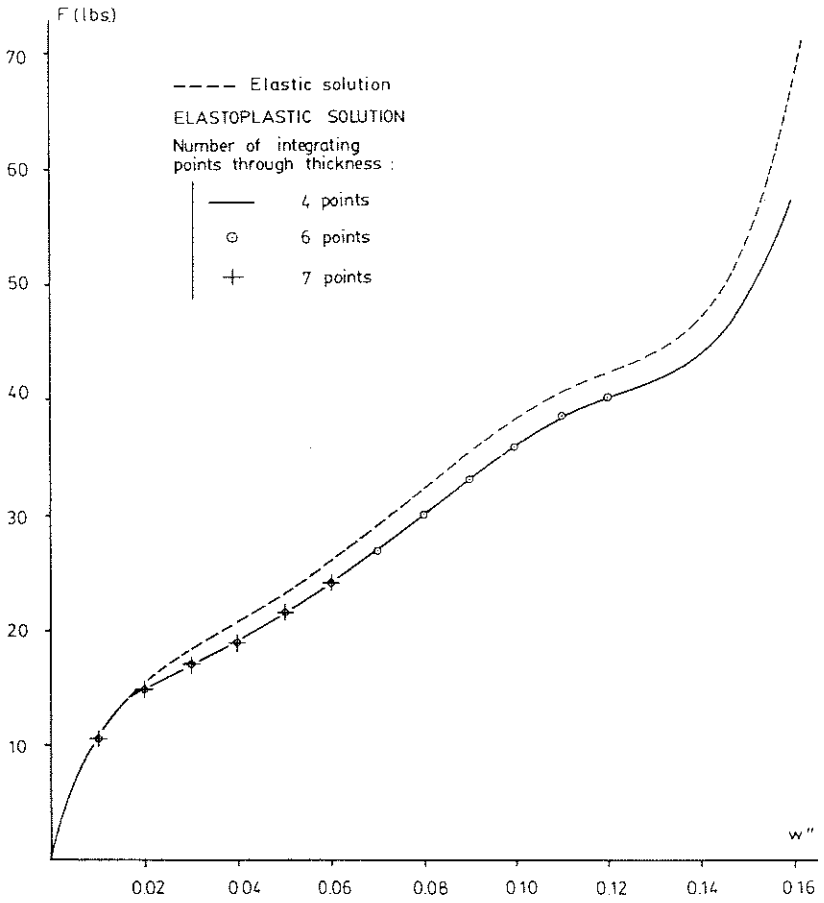

Figure 17. Spherical shell. Elastoplastic analysis. Plot of the central deflection versus load. Numerical results obtained with different integrating points through the shell thickness

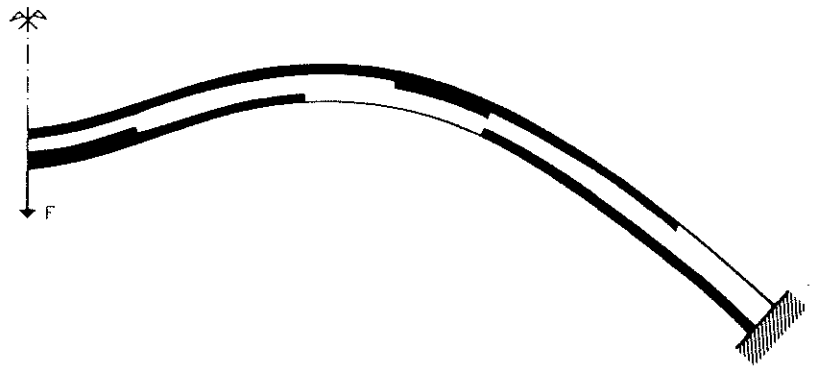

Figure 18. Spherical shell. Plastic zones for the maximum deflection of 0·16 in.

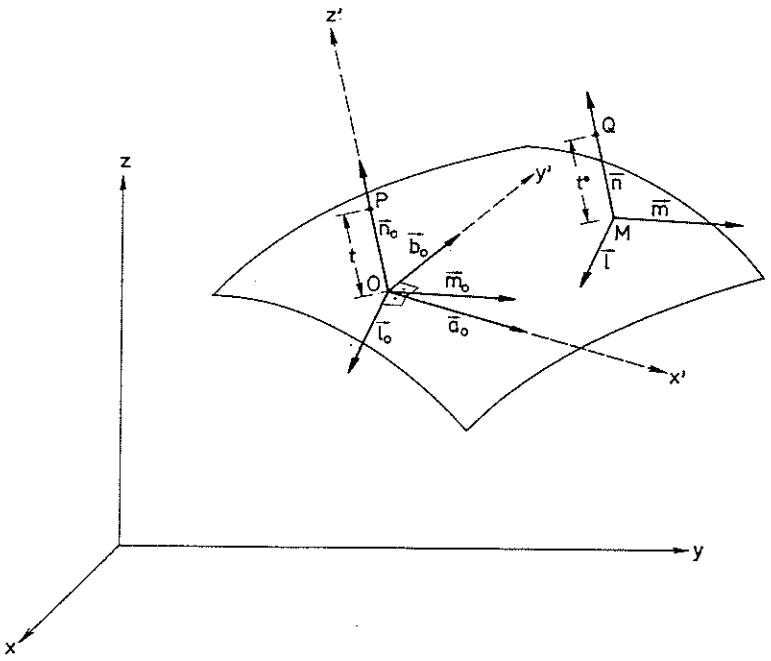

Figure 19.

where C_r and C_s are defined in equations (24) and (25), and subscript p refers to values in point P. It can also be found that

$$\mathbf{u}'_M = \mathbf{T}_0 \cdot \mathbf{u}_M \quad \text{and} \quad \mathbf{u}'_{1M} = \mathbf{T}_0 \cdot [\mathbf{l}, \mathbf{m}, \mathbf{n}] \cdot \bar{\mathbf{u}}_{1M} \tag{71}$$

where $\mathbf{u}_M$ and $\bar{\mathbf{u}}_{1M}$ denote components in the global system xyz and local vector system $\mathbf{l}\,\mathbf{m}\,\mathbf{n}$ (in point M), respectively, matrix $\mathbf{T}$ has been defined in equation (6) and subscript zero denotes values in point O.

Substituting equations (71) in (69) it is finally obtained that

$$\mathbf{u}'_Q = \mathbf{T}_0 \cdot \{\mathbf{u}_M + t^* [\mathbf{l}, \mathbf{m}, \mathbf{n}] \cdot \bar{\mathbf{u}}_{1M}\} \tag{72}$$

Differentiation of equation (72) and substitution in equation (70) (making $Q \to P$, $M \to \mathrm{O}$ and $t^* \to t$), yields

$$\begin{aligned} \mathbf{g}_1 &= C_r \mathbf{T} \frac{\partial \mathbf{u}_0}{\partial r} + C_r t \left[\bar{\mathbf{T}} \frac{\partial \bar{\mathbf{u}}_1}{\partial r} + \Delta_2 \bar{\mathbf{u}}_1 \right] \\ \mathbf{g}_2 &= C_s \mathbf{T} \frac{\partial \mathbf{u}_0}{\partial s} + C_s \cdot t \left[\bar{\mathbf{T}} \frac{\partial \bar{\mathbf{u}}}{\partial s} + \Delta_2 \bar{\mathbf{u}}_1 \right] \\ \mathbf{g}_3 &= \mathbf{T} \cdot \bar{\mathbf{u}}_1 \end{aligned} \tag{73}$$

where matrices $\bar{\mathbf{T}}$, Δ_1 and Δ_2 are defined in equations (9), (26) and (27). From equation (73) the operator $\mathbf{L}$ of equation (23) can be directly obtained.

APPENDIX II: COMPUTATION OF THE PRINCIPAL CURVATURE DIRECTIONS, RADIUS OF CURVATURE AND SHAPE FUNCTION DERIVATIVES

The isoparametric expression

$$\mathbf{r}_0 = \sum_1^{n_e} N_i(\xi, \eta)\mathbf{r}_{0i} \tag{74}$$

defines a parameteric form of the shell middle surface within each element for which the curvature directions and curvature radius can be calculated by simple application of formulae of differential calculus.[18]

Thus, let E, F, G and e, f, g be the coefficients of the fundamental expressions defining the shell surface, where

$$\begin{aligned} E &= \frac{\partial \mathbf{r}_0}{\partial \xi}\cdot\frac{\partial \mathbf{r}_0}{\partial \xi};\ F = \frac{\partial \mathbf{r}_0}{\partial \xi}\cdot\frac{\partial \mathbf{r}_0}{\partial \eta};\ G = \frac{\partial \mathbf{r}_0}{\partial \eta}\cdot\frac{\partial \mathbf{r}_0}{\partial \eta} \\ e &= \frac{1}{\sqrt{(EG-F^2)}}\cdot\frac{\partial^2 \mathbf{r}_0}{\partial \xi^2}\cdot\left(\frac{\partial \mathbf{r}_0}{\partial \xi}\times\frac{\partial \mathbf{r}_0}{\partial \eta}\right) \\ f &= \frac{1}{\sqrt{(EG-F^2)}}\cdot = \frac{\partial^2 \mathbf{r}_0}{\partial \xi \partial \eta}\cdot\left(\frac{\partial \mathbf{r}_0}{\partial \xi}\times\frac{\partial \mathbf{r}_0}{\partial \eta}\right) \\ \mathbf{g} &= \frac{1}{\sqrt{(EG-F^2)}}\cdot = \frac{\partial^2 \mathbf{r}_0}{\partial \eta^2}\cdot\left(\frac{\partial \mathbf{r}_0}{\partial \xi}\times\frac{\partial \mathbf{r}_0}{\partial \eta}\right) \end{aligned} \tag{75}$$

The equation

$$(Fg - Gg)\lambda^2 + (Eg - Ge)\lambda + (Ef - Fe) = 0 \tag{76}$$

where $\lambda = \delta\xi/\delta\eta$ yields values of λ_1 and λ_2, which define two orthogonal directions in which the curvature has a maximum and a minimum, respectively. Such curvatures can be obtained by

$$\begin{aligned} \frac{1}{R_1} &= \frac{f + g\lambda_1}{F + G\lambda_1} = \frac{e + f\lambda_1}{E + F\lambda_1} \\ \frac{1}{R_2} &= \frac{f + g\lambda_2}{F + G\lambda_2} = \frac{e + f\lambda_2}{E + F\lambda_2} \end{aligned} \tag{77}$$

The radius of curvature R_r and R_s are obtained as R_1 and R_2, respectively. The angles which the principal curvature directions form with the co-ordinate line ξ (which is easy to identify for each element, see Figure 20) are given by

$$\begin{aligned} \gamma &= \arccos\frac{E + \lambda_r E}{\sqrt{E}\sqrt{(E + 2\lambda_r F + \lambda_r^2 G)}} \\ \delta &= \gamma + \frac{\pi}{2} \end{aligned} \tag{78}$$

It is well known that there might exist points on the shell surface in which all curvature directions are principal and they have the same radius of curvature (umbilical points). In such points, the angles γ and δ have no particular meaning and they can be defined arbitrarily (in such cases, as happens with the problem of spherical shell, the curvature direction 'r' has been taken to coincide with local axis ξ).

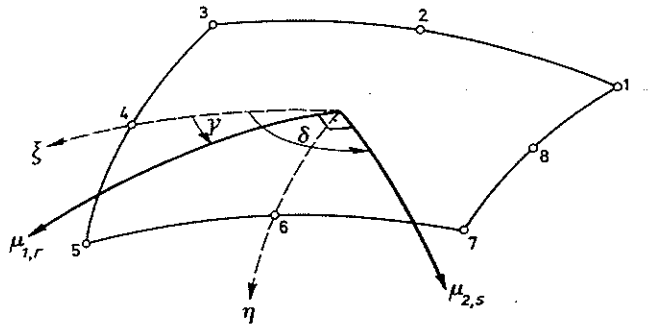

$$\delta = \nu + \frac{\pi}{2}$$

Figure 20.

It can be proved[12] that the derivatives of the shape functions with respect to the principal curvature directions are given by

$$\frac{\partial N_i}{\partial r} = \frac{\dfrac{\partial N_i}{\partial \xi} + \lambda_r \dfrac{\partial N_i}{\partial \eta}}{\sqrt{(|E + 2\lambda_r F + \lambda_r^2 G|)}}$$
$$\frac{\partial N_i}{\partial s} = \frac{\dfrac{\partial N_i}{\partial \xi} + \lambda_s \dfrac{\partial N_i}{\partial \eta}}{\sqrt{(|E + 2\lambda_s F + \lambda_s^2 G|)}} \tag{79}$$

Finally, vectors **a**, **b** and **n** can be evaluated from their definition shown in Figure 1 and equations (74) and (79).

APPENDIX III

Differentiation of the expressions of the components of vector $\mathbf{V}_i$ of equations (32) and (33) leads to

$$\frac{\partial \mathbf{V}_i^{\mathrm{T}}}{\partial \theta_{\bar{x}i}} = \begin{bmatrix} A_1 & A_2 & A_3 \\ A_2 & A_4 & A_5 \end{bmatrix}; \quad \frac{\partial \mathbf{V}_i^{\mathrm{T}}}{\partial \theta_{\bar{y}i}} = \begin{bmatrix} A_2 & A_4 & A_5 \\ A_4 & A_6 & A_7 \end{bmatrix}$$

where

$$A_1 = \frac{\partial V_{1i}}{\partial \theta_{\bar{x}i}} = -\frac{1}{e_i}\left[3\left(\frac{\cos\alpha_i}{\alpha_i} - \frac{\sin\alpha_i}{\alpha_i^2}\right)\sin^2\beta_i\cos\beta_i - \sin\alpha_i\cos^3\beta_i\right]$$

$$A_2 = \frac{\partial V_{2i}}{\partial \theta_{\bar{x}i}} = \frac{\partial V_{1i}}{\partial \theta_{\bar{y}i}} = -\frac{1}{e_i}\left[\left(\frac{\cos\alpha_i}{\alpha_i} - \frac{\sin\alpha_i}{\alpha_i^2}\right)(\sin^3\beta_i - 2\sin\beta_i\cos^2\beta_i)\right.$$

$$\left. - \sin\alpha_i\sin\beta_i\cos^2\beta_i\right]$$

$$A_3 = \frac{\partial V_{4i}}{\partial \theta_{\bar{x}i}} = -\cos\alpha_i \cos^2\beta_i - \frac{\sin\alpha_i}{\alpha_i}\sin^2\beta_i$$

$$A_4 = \frac{\partial V_{3i}}{\partial \theta_{\bar{x}i}} = \frac{\partial V_{2i}}{\partial \theta_{\bar{y}i}} = -\frac{1}{e_i}\left[\left(\frac{\cos\alpha_i}{\alpha_i} - \frac{\sin\alpha_i}{\alpha_i^2}\right)(\cos^3\beta_i - 2\sin^2\beta_i\cos\beta_i) - \sin\alpha_i \sin^2\beta_i \cos\beta_i\right]$$

$$A_5 = \frac{\partial V_{5i}}{\partial \theta_{\bar{x}i}} = \frac{\partial V_{4i}}{\partial \theta_{\bar{y}i}} = \left(\frac{\sin\alpha_i}{\alpha_i} - \cos\alpha_i\right)\sin\beta_i\cos\beta_i$$

$$A_6 = \frac{\partial V_{3i}}{\partial \theta_{\bar{y}i}} = -\frac{1}{e_i}\left[3\left(\frac{\cos\alpha_i}{\alpha_i} - \frac{\sin\alpha_i}{\alpha_i^2}\right)\sin\beta_i\cos^2\beta_i - \sin\alpha_i\sin^3\beta_i\right]$$

$$A_7 = \frac{\partial V_{5i}}{\partial \theta_{\bar{y}i}} = -\cos\alpha_i \sin^2\beta_i - \frac{\sin\alpha_i}{\alpha_i}\cos^2\beta_i$$

REFERENCES

1. S. Ahmad, B. M. Irons, and O. C. Zienkiewicz, 'Analysis of thick and thin shell structures by curved elements', *Int. j. numer. methods eng.* **2**, 419–451 (1970).
2. J. H. Argyris, H. Balmer, M. Kleiber and U.Hindenlang, 'Natural description of large inelastic deformations for shells of arbitrary shape—applications of trump element', *Computer Meth. Appl. Mech. Eng.*, **22**, 361–389 (1980).
3. J. H. Argyris and S. Symeonidis, 'Non-linear finite element analysis of elastic systems under non-conservative loading—natural formulation', *J. Comp. Meth. Appl. Mech. Eng.*, **26**, 75–123 (1981).
4. T. Y. Chang and K. Sawamiphakdi, 'Large deflection and post-buckling analysis of shell structures', *Comp. Meth. Appl. Mech. Eng.*, **32**, 311–326 (1982).
5. J. S. Doltsinis, K. Straub and K. J. William (eds.), *Proc. of the 2nd Int. Conf. on Finite Elements in Nonlinear Mechanics*, Stuttgart, North-Holland, Amsterdam, 1981.
6. J. R. Hughes and W. K. Liu, 'Non-linear finite element analysis of shells—part I. Three-dimensional shells', *Comp. Meth. Appl. Mech. Eng.*, **26**, 331–362 (1981).
7. J. R. Hughes and W. K. Liu, 'Non-linear finite element analysis of shells—part II. Two-dimensional shells', *J. Comp. Methh. Appl. Mech. Eng.*, **27**, 167–181 (1981).
8. M. Kleiber, J. A. König and A. Sawczuk, 'Studies on plastic structures: stability, anisotropic hardening, cyclic loads', *J. Comp. Meth. Appl. Mech. Eng.*, **33**, 487–556 (1982).
9. S. Lewis, 'Bending of rectangular plates with large deflections', *N.A.C.A Tech. Note 846* (1942).
10. R. D. Mindlin, 'Influence of rotatory inertia and shear on flexural motion of isotropic elastic plates', *J. Appl. Mech.*, **18**, 31–38 (1951).
11. G. Ch. Nayak, 'Plasticity and large deformation problems by the finite element method', *C/Ph/15/71*, University of Wales, Swansea, U.K. (1971).
12. J. Oliver, 'Una formulación cuasi-intrinseca para el estudio, por el método de los elementos finitos de vigas, arcos, placas y láminas sometidos a grandes corrimientos en régimen elastoplástico' (in spanish), *Ph.D. thesis*, E. T. S. Ingenieros de Caminos, Universidad Politécnica, Barcelona, Spain (1982).
13. E. Oñate, E. Hinton and N. Glover, 'Techniques for improving the performance of Ahmad shell elements', Proc. World Congress IASS, Madrid, Spain (1979).
14. D. R. J. Owen and E. Hinton, *Finite Elements in Plasticity*, Pineridge Press, Swansea, U.K. 1980.
15. A. Pica, R. D. Wood and E. Hinton, 'Finite element analysis of geometrically non-linear plate behaviour using a Mindlin formulation', *C/R/332/78*, University of Wales, Swansea, U.K. (1978).
16. E. Ramm, 'A plate/shell element for large deflections and rotations', in *Formulations and Computational Algorithms in Finite Element Analysis* (Eds. K. J. Bathe, J. T. Oden and W. Wunderlich), M.I.T. Press, 1977.
17. A. B. Sabir and A. C. Lock, 'The application of finite elements to the large deflection geometrically non-linear behaviour of cylindrical shells', in *Variational Methods in Engineering*, Vol. 7 (Eds. Brebbia and Tottenham), Southampton Univ. Press, 1973, pp. 66–75.
18. D. J. Struik, *Lectures on Classical Differential Geometry*, Addision-Wesley, Massachusetts, 1961.
19. K. S. Surana, 'Geometrically non-linear formulation for the curved shell elements', *Int. J. Num. Meth. Engng*, **19**, 581–615 (1983).
20. K. Washizu, *Variational Methods in Elasticity and Plasticity*, 2nd edn, Pergamon Press, Oxford and New York, 1975, pp. 182–203.

21. R. D. Wood, 'The application of finite element methods to geometrically non-linear structural analysis', *C/Ph/20/73*, University of Wales, Swansea, U.K. (1973).
22. R. D. Wood and O. C. Zienkiewics, 'Geometrically non-linear finite element analysis of beams, frames, arches and axisymmetric shells', *Comput. Struct.*, **7**, 725–735 (1977).
23. O. C. Zienkiewicz and G. C. Nayak, 'A general approach to problems of large deformation and plasticity using isoparametric elements', 3rd. Conf. on Matrix Methods in Struct. Mech., A.F.I.T, Wright–Patterson, Ohio (Oct. 1971).
24. O. C. Zienkiewicz, *The Finite Element Method*, McGraw-Hill, New York, 1979.
25. M. A. Crisfield, 'Incremental iterative solution procedure for non-linear structural analysis', *Proceedings of the International Conference on Numerical Methods for Non-Linear Problems*, Pineridge Press, Swansea, U. K., 1980.
26. B. H. Kröplin and D. Dinkler, 'A creep type strategy used for tracing the load path in elastoplastic post buckling analysis', *Proceedings of the 2nd International Conference on Finite Elements in Nonlinear Mechanics*, Stuttgart, North-Holland, Amsterdam, 1981.
27. E. D. L. Pugh, E. Hinton and O. C. Zienkiewicz, 'A study of quadrilateral plate bending elements with reduced integration', *Int. j. numer. methods eng.*, **12**, 1059–79 (1978).